Applied Catalysis B: Environmental 123–124 (2012) 405–413

Contents lists available at SciVerse ScienceDirect

Applied Catalysis B: Environmental

journal homepage: www.elsevier.com/locate/apcatb

Support mediated promotional effects of rare earth oxides (CeO_2 and La_2O_3) on N_2O decomposition and N_2O reduction by CO or C_3H_6 over Pt/Al_2O_3 structured catalysts

M. Konsolakis **, C. Drosou, I.V. Yentekakis *

Laboratory of Physical Chemistry and Chemical Processes, Department of Sciences, Technical University of Crete, 73100 Chania, Crete, Greece

ARTICLE INFO

Article history:
Received 26 March 2012
Accepted 28 April 2012
Available online 5 May 2012

Keywords:
N_2O decomposition
Platinum
Rare earth oxides
CeO_2
La_2O_3
Cordierite monoliths
DRIFTS

ABSTRACT

The N_2O decomposition and reduction by CO or C_3H_6 over rare earth oxides (REOs)-modified Pt/Al_2O_3 structured catalysts, *i.e.*, coated on ceramic honeycomb monoliths, were comparatively investigated in a wide temperature interval of 100–600 °C, either in the presence or in the absence of excess O_2 and H_2O. It was shown that the de-N_2O efficiency can be remarkably enhanced *via* modification of Al_2O_3 support with rare earth oxides (REOs). In specific, complete conversion of N_2O can be attained over REOs-modified catalysts at a relatively low temperature (*ca.* 480 °C) even in the presence of excess O_2, which in general depresses de-N_2O efficiency, in opposite to the unmodified Pt/Al_2O_3 catalyst, over which, 20% N_2O conversion is never exceeded for temperatures up to 600 °C. In terms of turnover frequency (TOF), optimally modified (by REOs) $Pt–Al_2O_3$ catalyst exhibits one order of magnitude higher activity compared to that of the unpromoted Pt/Al_2O_3 sample. Under reducing conditions the N_2O conversion is strongly enhanced by C_3H_6 and especially by CO, whereas marginal inhibition is induced by reducing agents under excess oxygen conditions. Water was found to induce a detrimental influence on N_2O decomposition, with its effect however, to be partially reversible. An *in situ* diffuse reflectance infrared Fourier transform spectroscopic (DRIFTS) study, using CO as a probe molecule, was performed over both unmodified and REOs-modified Pt/Al_2O_3 catalysts to correlate their surface characteristics with their de-N_2O efficacy. The results revealed that the superior catalytic performance of promoted samples could be mainly attributed to the increase of Pt dispersion as well as to the development of Pt sites with exceptional electron density, located on the metal–support interfacial area.

1. Introduction

Nitrogen oxides (NOx) abatement from industrial exhaust gases constitutes a subject of major environmental importance [1,2]. Lately, considerable efforts have been also devoted on nitrous oxide (N_2O) emission control, due to its harmful impact on stratospheric ozone depletion and its outstanding Global Warming Potential (GWP) which is about 310 and 21 times greater than that of CO_2 and CH_4, respectively [1–7].

Although, the atmospheric concentration of N_2O remained relatively constant until the pre-industrial period (~275 ppbv), nowadays N_2O levels are significantly increased (~310 ppbv) due to anthropogenic activities including, among others, the use of fertilizers in land cultivation, stationary and mobile combustion processes and industrial manufacturing of nitric and adipic acids [1]. The negative impact of N_2O on the environment in combination with its rapid increase in the atmosphere, forced the United Nations Framework Convention on Climate Change in Kyoto (1997) to include N_2O, along with CO_2, CH_4, HFCs, PFCs and SF_6, in the gases the emissions of which should be reduced by at least by 5% during the period 2008–2012 in reference to 1990 levels, with a goal of further decrease up to 20% in 2020 [1,3,5]. To accomplish this target the control of N_2O emissions from combustion processes' off-gases is of great importance [1,3].

The catalytic decomposition of N_2O into N_2 consists one of the most efficient technologies for N_2O abatement. So far, various types of catalysts such as supported noble metals [8–13], metal oxides [14,15], spinels [16,17] and zeolites [18,19] have been reported to exhibit satisfactory activity for N_2O decomposition. However, most of these de-N_2O catalytic systems suffer from O_2 poisoning; strongly chemisorbed oxygen atoms on active catalyst sites, originating either from gas phase or from N_2O decomposition, progressively leads to catalyst self-poisoning [1–3]. Compared to other catalytic systems, noble metal supported catalysts exhibit better

* Corresponding author. Tel.: +30 28210 37752; fax: +30 28210 37843.
** Corresponding author.
E-mail addresses: mkonsol@science.tuc.gr (M. Konsolakis), yyentek@science.tuc.gr (I.V. Yentekakis).

0926-3373/$ – see front matter © 2012 Elsevier B.V. All rights reserved.
http://dx.doi.org/10.1016/j.apcatb.2012.04.048

activity for N_2O decomposition especially at low temperatures [2]. In particular, Rh based catalysts are among the most active for de-N_2O process; however, the formation of inactive Rh_2O_3 phase under oxidizing conditions [20] in combination with the high cost of Rh metal compose the main restrictive factors for its practical application. On the other hand, the N_2O decomposition over Pt catalysts is drastically hindered by adsorbed oxygen leading to complete deactivation on a fully oxidized Pt surface [9,21]. To this end, considerable efforts have been recently focused on enhancing the catalytic properties of noble metals by surface or structural modifiers such as alkalis [22–25] and REOs [26,27]. Moreover, the use of reducing agents such as CO and hydrocarbons, which are also components of industrial exhaust gases, could facilitate the removal of strongly adsorbed oxygen atoms, overcoming the oxygen poisoning [28].

Regarding structural modifiers, cerium oxide is by far the most frequently used material. Ceria is mainly used as a washcoat constituent in three way catalytic converters (TWCs), due to its unique acid–base and redox properties which can enhance both the catalytic activity of metal sites and the stability of support materials [29]. Although the main promoting effect of cerium oxide has been ascribed to its high oxygen storage capacity, recent studies are also focused on the influence of ceria to the electronic state and the concomitant catalytic activity of metal sites interfaced with CeO_2 [26,30–32]. La_2O_3 is also considered as a promising promoter/stabilizer in several catalytic systems since it has shown significant improvements on the stabilization of Al_2O_3 support and on the noble metals' dispersion and their catalytic activity [33]. In this respect, in a previous study concerning the role of Ce, Zr and La as structural stabilizers/promoters of Pt/Al_2O_3 TWCs, it has been found that an amount of 2–4 wt% of La_2O_3 in the washcoat is beneficial for both catalytic performance and thermal durability [34]. The pronounced effect of La was mainly ascribed to an enhancement of ceria based mixed oxides' reducibility, which in turn alters the activity of metal sites *via* metal–support interactions [34].

Given that the N_2O decomposition is notably affected by the electronic properties of catalyst surface [23] as well as by the desorption or scavenging rate of adsorbed oxygen atoms [21,22], it is reasonably expected that REOs, which can modify both the oxidation state of metal sites and the mobility of oxygen atoms, can play an essential key role on de-N_2O process. In addition, taking into account that the majority of N_2O decomposition studies have been performed with catalysts in the form of inapplicable powders [2], it is of particular interest to investigate the de-N_2O process in practical configurations, such as cordierite monoliths, that offer, among other advantages, the opportunity to treat large gas volumes with insignificant pressure drop [35–40].

Considering the aforementioned aspects, *i.e.* the significant influence of REOs on catalysts' structural and surface behavior, as well as the requirement of structured catalysts suitable for practical applications, the current work aims: to investigate the de-N_2O catalytic performance of structured Pt/Al_2O_3–(CeO_2–La_2O_3) catalysts; to elucidate the effect of CeO_2 and La_2O_3 washcoat modifiers on the surface chemistry of Pt and its correlation with de-N_2O processes, involving also the influence of operational parameters, *i.e.*, excess O_2, water steam and/or reducing agents (CO or C_3H_6) on the overall de-N_2O catalytic efficiency.

2. Experimental

2.1. Preparation of washcoated monoliths

The co-precipitation method was followed to synthesize bare Al_2O_3, CeO_2-modified Al_2O_3 and CeO_2/La_2O_3-modified Al_2O_3 supporting materials. To this end, a solution of NH_4OH was added dropwise at room temperature to a stirring solution containing the desirable amounts of $Ce(NO_3)_3{\cdot}6H_2O$, $La(NO_3)_3{\cdot}6H_2O$ and $Al(NO_3)_3{\cdot}9H_2O$ precursor materials until the pH of the solution reached the value of ~10. The resultant participates were dried overnight at 110 °C and calcined at 600 °C for 2 h. Addition of noble metal (Pt) to supporting materials was performed by impregnating the support to an aqueous solution of $Pt(NH_3)_2(NO_2)_2$ with the appropriate concentration so as to yield 0.5 wt% Pt loading. The resulted suspensions were dried in air at 110 °C overnight and then calcined at 600 °C for 2 h.

Cylindrical cordierite samples (manufactured by Corning, USA) with 400 square cells/in.^{2} and typical dimensions of about 20 mm diameter and 10 mm length (~3.3 cm^3 vol.%), were immersed for 1 min in a stirring slurry containing ~15 wt% of washcoating powders. Subsequently, the cordierite samples were withdrawn and dried at 110 °C for 2 h. This procedure was repeated until the desired percentage of 20 ± 0.5 wt% washcoat was obtained. The resulted monoliths, with a total weight of 2.2 ± 0.1 g, were finally calcined at 600 °C for 2 h. The textural, morphological and surface characterization were carried out over the remaining slurries imposed to the same pre-treatment (calcination at 600 °C for 2 h) with the washcoated monoliths. The classification of prepared monoliths along with their constitution is summarized in Table 1.

2.2. Catalyst characterization

Determination of adsorption–desorption isotherms was carried out at −196 °C using the Nova 2200e Quantachrome flow apparatus. BET surface areas were determined according to the Brunauer–Emmett–Teller (BET) method in the relative pressure range of 0.05–0.30. The total pore volumes were obtained from the volume of nitrogen adsorbed at the highest relative pressure whereas the average pore size diameters were estimated by the Barrett–Joyner–Halenda (BJH) method. Prior to the measurements the samples were degassed at 350 °C for 5 h under vacuum. Pt dispersions are evaluated by a DRIFTS-aided method based on CO chemisorption, described in detail in a previous communication [41]. The physicochemical characteristics of washcoated composites are also included in Table 1.

2.3. Catalytic performance evaluation

Catalytic experiments were carried out in a continuous flow reactor consisted of a quartz tube, 300 mm long with an inner diameter of 24 mm, encased in a tubular furnace. The monolithic specimen was put in the middle of the reactor, whereas its temperature was measured with a centered K-thermocouple. The space between monolithic sample and reactor walls is covered by quartz fiber-glass, inert to reaction mixture.

High pressure cylinders with certified standard gas mixtures of 5% N_2O, 10.1% CO, 10% C_3H_6, 20.7% O_2 and 20% H_2 in He and ultrapure He (99.999%) were used to provide the desired reactants feed mixture in a mixing unit *via* a series of independent mass flow controllers; the reactants' mixture was then supplied to the reactor at 1 bar. The feed composition employed during N_2O catalytic decomposition experiments was 0.1% N_2O, 0 or 2% O_2 balanced with He. The effect of 0.1% CO or 0.1% C_3H_6 on N_2O reduction rate was also investigated either in the presence or in the absence of O_2 in the feed composition. The influence of H_2O-steam on N_2O decomposition was investigated by passing the reaction mixture through a thermostatically controlled water-steam saturator, placed before the reactor, in order to enrich the flux with 3% H_2O. The total gas flow rate was 550 cm^3(STP)/min corresponding to a Gas Hourly Space Velocity (GHSV) of 10,000 h^{-1} (a value matching the range existed in combustion facilities [40]). Before catalytic evaluation measurements, all monoliths were *in situ* pretreated at identical conditions involving H_2 flow (20% in He) for 1 h at 400 °C, followed

Table 1
Monoliths' constitution and physicochemical characteristics of washcoating materials.

Monoliths' code	Monoliths' constitution (wt%)					Washcoats' physicochemical properties				
	Pt	Al_2O_3	CeO_2	La_2O_3	Ceramic substrate	Pt dispersion (%)	Pt mean crystallize size[a] (nm)	BET surface area (m^2/g)	Total pore volume (cm^3/g)	Mean pore diameter (nm)
Pt/Al	0.1	19.9	–	–	80	14	9.8	200	0.42	8.44
Pt/Al–Ce	0.1	15.9	4.0	–	80	81	1.7	195	0.36	7.46
Pt/Al–CeLa	0.1	15.9	3.2	0.8	80	93	1.5	192	0.35	7.28

[a]Calculations based on Pt surface atom density of 1.53×10^{19} atoms/m^2 [41].

with He flow for 1 h at the same temperature. Subsequently, the monolithic sample is cooled down under He flow to room temperature and the reaction gas mixture is fed to the reactor. The de-N_2O performance of monolithic specimens was evaluated by increasing the reactor temperature stepwise from room temperature to 600 °C and held constant at each temperature for at least 30 min prior taking measurements. Analysis of the reaction products was carried out using on-line Gas Chromatography (Shimatzu-14B) equipped with Porapak N and Molecular Sieve 5A columns.

Intrinsic N_2O decomposition activity of the catalysts is also estimated, in terms of turnover frequency, TOF (molecules of N_2O decomposed per Pt surface atom per second):

$$\mathrm{TOF}(s^{-1}) = \frac{F_{N_2O} \times X_{N_2O}}{N_{Pt}}$$

where F_{N_2O} is the N_2O flow rate (mol N_2O/s), X_{N_2O} is the conversion of N_2O and N_{Pt} is the number of moles of surface Pt atoms. In order to ensure the absence of mass and heat transfer limitations, TOF values are estimated using only data corresponding to N_2O conversions lower than ~15%.

2.4. DRIFTS studies of CO adsorption

The influence of CeO_2 and La_2O_3 on the chemisorptive properties of Pt/Al_2O_3 catalysts was investigated by means of *in situ* DRIFT spectroscopy using CO as probe molecule. Diffuse reflectance IR spectra were collected using an Excalibur spectrometer FTS 3000, equipped with an MCT detector cooled by liquid nitrogen and an IR cell (Specac, Environmental Chamber DRIFT model) designed for *in situ* sample treatment. Infrared spectra were obtained with resolution of 2 cm^{-1} and accumulation of 64 scans. During IR measurements the external optics were purged with CO_2-free dry air generated from an air purifier system (Claind Italy, CO_2-PUR model). Catalyst samples in a powder form (~80 mg), representative of washcoating materials, were placed into the IR cell and carefully flattened in order to optimize the intensity of the reflected IR beam.

Samples' pretreatment before adsorption experiments involves the following steps: (i) heating to 400 °C under He flow, (ii) reduction with 20% H_2 at 400 °C for 1 h, (iii) purging with He at 400 °C for 30 min, (iv) cooling down to room temperature under He flow and background spectra acquisition at each desired temperature. After this, CO (0.5% in He) is introduced in the IR cell at room temperature (25 °C) and spectra are recorded until steady state (saturation of Pt sites with CO). Then the gas phase is evacuated and the infrared spectrum is collected, corresponding to IR spectrum of adsorbed CO at 25 °C. The thermal stability of adsorbed species is evaluated by spectra acquisition under He flow in the temperature interval of 25–450 °C. The total flow rate during IR experiments is maintained at 80 cm^3/min.

3. Results and discussion

3.1. Effect of REOs on washcoats' physicochemical characteristics

The physicochemical characteristics (BET surface area, total pore volume, average pore size diameter, dispersion and mean crystallite size) of catalytic samples used as monoliths' washcoats are depicted in Table 1. It is obvious that the un-modified Pt/Al sample possess the highest value of BET surface area (200 m^2/g) and total pore volume (0.42 cm^3/g). Incorporation of REOs on Al_2O_3 support results to slightly lower BET area and total pore volume values. However, the Pt dispersion is significantly increased from 14% over the un-modified Pt/Al sample to 81 and 93% over the CeO_2-modified (Pt/Al–Ce) and $CeO_2 + La_2O_3$-modified (Pt/Al–CeLa) samples, respectively, indicating the beneficial effect of both CeO_2 and La_2O_3 on noble metal dispersion, as discussed in detail elsewhere [34]. This pronounced effect of REOs on Pt dispersion results to Pt nanoparticles with an average size lower than 2 nm, in contrast to much higher size (~10 nm) obtained over the unpromoted sample (Table 1).

3.2. Effect of REOs on N_2O decomposition

Fig. 1 depicts the N_2O conversion (dark symbols, solid lines) as a function of temperature for the un-modified (Pt/Al), CeO_2-modified (Pt/Al–Ce) and $CeO_2 + La_2O_3$-modified (Pt/Al–CeLa) monolithic samples listed in Table 1. In the same figure the influence of 2% O_2 is also depicted (open symbols, dashed lines), in order to assess the effect of excess oxygen on N_2O decomposition. It is obvious that the unmodified Pt/Al sample exhibits the inferior de-N_2O

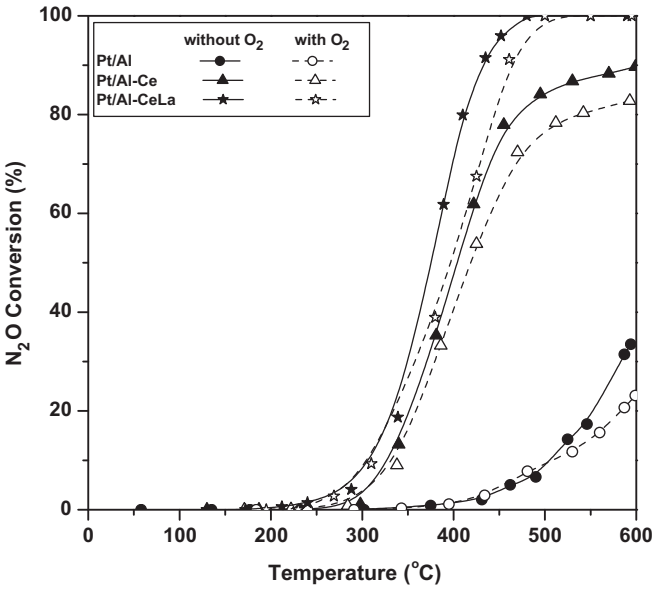

Fig. 1. N_2O conversion in the absence or presence of O_2 over the monolithic samples listed in Table 1. Reaction conditions: 0.1% N_2O, 0 or 2% O_2, GHSV = 10,000 h^{-1}.

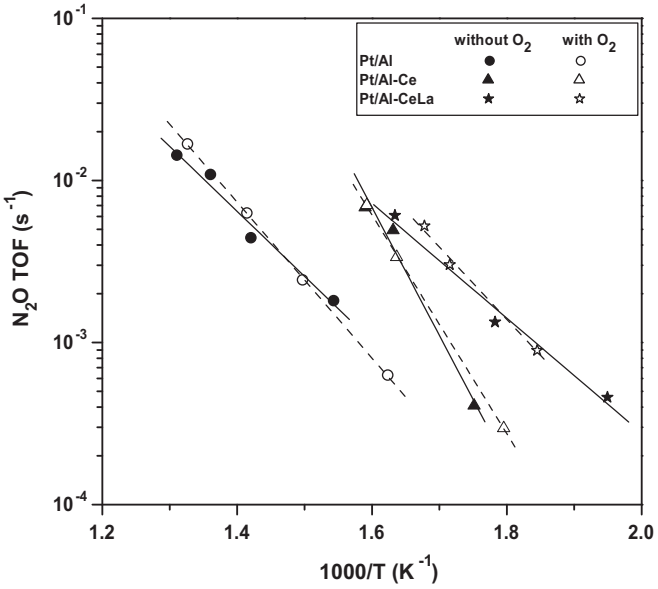

Fig. 2. Turnover frequencies (TOF) of the N_2O decomposition over the monolithic samples listed in Table 1. Reaction conditions: 0.1% N_2O, 2% O_2, GHSV = 10,000 h^{-1}.

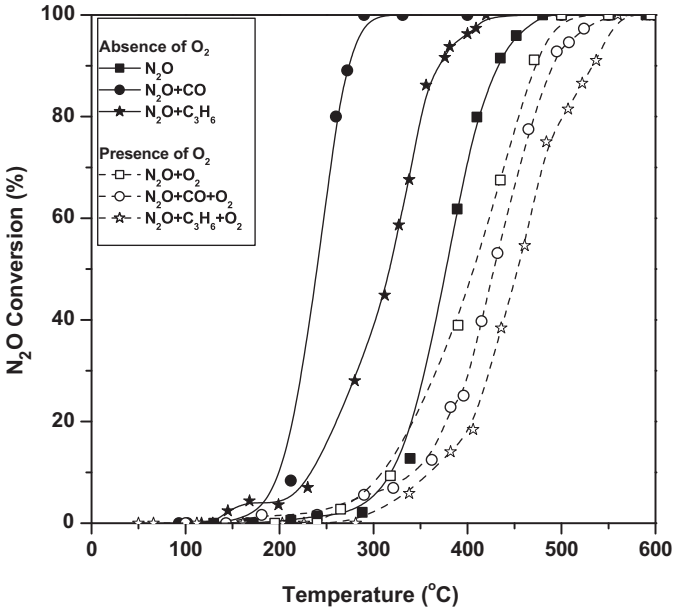

Fig. 3. Effect of reducing agents (CO or C_3H_6) on N_2O decomposition in the absence or presence of O_2 over Pt/Al–CeLa monolithic sample. Reaction conditions: 0.1% N_2O, 0 or 2% O_2, 0.1% CO or 0.1% C_3H_6, GHSV = 10,000 h^{-1}.

performance offering a maximum conversion of ~35% at 600 °C under O_2-free feed. This inferior performance is further inhibited by O_2; N_2O conversion of ~20% is obtained at 600 °C under O_2-containing feed. However, incorporation of CeO_2 on Al_2O_3 support (Pt/Al–Ce sample) drastically improves the catalytic performance resulting in 90% N_2O conversion at 600 °C and in a *light-off* temperature (*i.e.*, temperature for 50% conversion, T_{50}) of about 405 °C under O_2-free feed. This enhanced N_2O decomposition performance is slightly hindered by excess oxygen in the feed, giving a maximum conversion of 83% at 600 °C and a T_{50} of 420 °C at these conditions. Interestingly, incorporation of both CeO_2 and La_2O_3 oxides on Al_2O_3 support (Pt/Al–CeLa sample) further enhances the de-N_2O efficiency: In the absence of oxygen, 100% N_2O conversion can be obtained at 480 °C, whereas T_{50} is about 30 °C lower (375 °C) compared to Pt/Al–Ce sample; a small inhibition is again induced by oxygen presence in the feed, shifting the N_2O conversion profile to slightly higher temperatures ($\Delta T \sim 20$–30 °C).

To gain insight into the effect of CeO_2 and La_2O_3 on intrinsic activity of catalysts, the turnover rates (TOF) of N_2O decomposition are depicted as a function of $1/T$ (Arrhenius plot, Fig. 2). The results clearly demonstrate the superior activity of Pt/Al–CeLa monolith, which exhibit up to 3- and 10-fold enhancement in N_2O consumption rate, in respect to Pt/Al–Ce and Pt/Al monoliths, respectively. It is worth noticing that the TOF values obtained for Pt/Al–CeLa sample are among the highest reported for N_2O decomposition in the presence of O_2 [*e.g.* 42, 43].

For comparison purposes the de-N_2O performance of the most effective Pt/Al–CeLa sample is comparatively presented in Table 2, along with that of literature reported structured catalysts (*i.e.* catalysts in monolithic form) tested for N_2O decomposition. (Comparison of the present results with that attained over catalysts in powder form is not attempted due to the differences in material shape and operation conditions.) It is worth noticing that the conversion performance of our catalyst with (CeO_2 + La_2O_3)-modified Pt/Al_2O_3 washcoat is favorably compared with that of other similarly structured catalysts despite the fact that most of the latter contain much higher noble metals loading and/or involve Rh as active phase (Rh is generally considered as one of the most active metals for N_2O decomposition).

3.3. *Effect of reducing agents (CO, C_3H_6) on N_2O decomposition*

Given that carbon monoxide and hydrocarbons are present in off-gases of most combustion processes, their effect on N_2O decomposition are studied under both reducing and oxidizing conditions, over the optimal Pt/Al–CeLa sample; both the effectiveness and the mechanism of action of the reducing agent, in the presence or absence of excess oxygen, are under consideration.

Fig. 3 depicts the effect of CO and C_3H_6 on N_2O decomposition in the presence or absence of O_2. As it can be observed addition of the reducing agent in an O_2-free reaction mixture considerably improves the catalytic performance, shifting the N_2O conversion profiles to notably lower temperatures, in comparison to that obtained in the case of direct N_2O decomposition. Specifically, in the presence of CO, 100% N_2O conversion can be achieved at temperatures as low as 290 °C instead of 480 °C required without CO. The corresponding temperature in the case of C_3H_6 is 420 °C, implying the superior performance of CO as reducing agent. However, in the presence of excess O_2 the use of a reducing agent (CO or C_3H_6) has a reverse effect on de-N_2O process, shifting N_2O conversion profiles to higher temperatures for both CO and C_3H_6; the negative effect being more intense for the latter. Concluding, CO or C_3H_6 has a positive impact on de-N_2O process only under reducing conditions.

The role of CO and O_2 on de-N_2O process can be better realized on the basis of Fig. 4, which depicts both N_2O and CO conversions either in the presence or in the absence of oxygen in the feed. It is evident that when oxygen is not fed, CO and N_2O conversion profiles totally coincide, both attaining 100% conversions at ~250 °C; this implies that CO oxidation proceeds *via* adsorbed oxygen atoms (O_{ads}) originating from N_2O decomposition. However, in the presence of oxygen in the feed, carbon monoxide is completely oxidized by gas phase oxygen derived O_{ads} at very low temperatures (*ca.* 80 °C), whereas the N_2O conversion initiates at much higher temperatures and is completed at ~550 °C.

Similar observations can be pointed out when C_3H_6 is used as reducing agent (Fig. 5). The fact that N_2O conversion initiates at far higher temperatures than those of complete elimination of the reducing agent (CO or C_3H_6; Figs. 4 and 5), in connection with the

Table 2
Comparison of de-N_2O performance of structured catalysts (T_{50}: temperature for 50% N_2O conversion; X_{500}: N_2O conversion at 500 °C).

Structured (monolithic) catalysts	Metal loading (wt.%)	GHSV (h^{-1})	Feed composition	T_{50} (°C)	N_2O conversion at 500 °C X_{500} (%)	Reference
Pt/Al_2O_3	0.1	10,000	0.1% N_2O	–	10	This
Pt/Al_2O_3–CeO_2	0.1	10,000	0.1% N_2O	405	85	work
Pt/Al_2O_3–CeO_2–La_2O_3	0.1	10,000	0.1% N_2O	375	100	
Pt/Al_2O_3–CeO_2–La_2O_3	0.1	10,000	0.1% N_2O + 2% O_2	400	100	
Ir/Al_2O_3–CeO_2	0.2	25,000	0.61% N_2O	540	25	[35]
Fe–Ir/Al_2O_3–CeO_2	1.5(Fe) + 0.2(Ir)	25,000	0.61% N_2O	470	80	
Ni–Rh/Al_2O_3–CeO_2	1.5 (Ni) + 0.2(Rh)	25,000	0.61% N_2O	480	80	
Ni–Rh/Al_2O_3–CeO_2	1.5 (Ni) + 0.2(Rh)	25,000	0.61% N_2O + 0.76%O_2	500	50	
Rh/TiO_2	0.07	10,000	0.06%N_2O	415	95	[36]
Rh/TiO_2	0.2	10,000	0.06%N_2O	380	95	
Rh/TiO_2	0.2	10,000	0.06%N_2O + 2%O_2	410	95	
Rh/Al_2O_3	0.8	8600	0.05%N_2O	320	100	[37]
Rh/Al_2O_3	0.8	8600	0.05%N_2O + 2%O_2	320	100	
Rh/Al_2O_3	0.4	8600	0.05%N_2O + 2%O_2	355	100	
Rh/Al_2O_3	0.2	8600	0.05%N_2O + 2%O_2	385	100	
$LaCoO_3/Al_2O_3$	6.0	10,000	0.5%N_2O	490	55	[38]
$LaCoO_3/Al_2O_3$	6.0	10,000	0.5%N_2O + 5%O_2	510	45	
Fe-mordenite	Not referred	30,000	0.5%N_2O + 5%O_2	540	25	[39]
Fe-ZSM-5	0.4	6000	0.05%N_2O + 6%O_2	425	100	[40]

sigmoid N_2O and CO (or C_3H_6) conversion patterns recorded under excess oxygen conditions, weakens the possibility of any direct interaction of N_2O with the reducing agent on the catalyst surface; in such a case a volcano type pattern may be expected for N_2O conversion with a maximum at the temperature where 100% conversion of the reducing agent is attained; such volcano behavior has been obtained for NO conversion during SCR of NO by hydrocarbons, manifesting the direct interaction between the reactants in that case [*e.g.* 44].

The preferential oxidation of CO by gas phase oxygen derived O_{ads} species instead of that originating from N_2O dissociation is more evident in Fig. 6 which depicts the variation of O_2 concentration along with CO and N_2O conversions during the N_2O + CO reaction in the presence of a small excess of O_2 (1500 ppm). It is obvious that at low temperatures CO is rapidly oxidized *via* gas phase oxygen whereas at higher temperatures, where N_2O decomposition initiates, the oxygen concentration is being increased. It is also evidenced from this data that N_2O dissociation is the dominant route for N_2O abatement even in the presence of CO.

The results of Figs. 4–6 also demonstrate the potential use of our REOs-modified catalysts as alternative materials for low temperature CO and/or VOCs abatement; complete elimination of CO and C_3H_6 is attained at 80 °C and 200 °C respectively.

The beneficial effect of the reducing agent on de-N_2O processes *via* the mechanism of O_{ads} scavenging described above is further evidenced in Fig. 7, which depicts the N_2O conversion as a function of CO/N_2O feed ratio at a constant temperature (330 °C). It is obvious that N_2O conversion is linearly increased up to 100% at $CO/N_2O = 1$, which corresponds to the stoichiomentric amount of CO required for complete removing of O_{ads} derived form N_2O dissociation. At higher CO/N_2O ratios N_2O conversion remains constant at 100%.

3.4. Effect of water on N_2O decomposition

Fig. 8 demonstrates the influence of 3% H_2O on N_2O conversion at a constant temperature of 500 °C. The catalyst is initially exposed to a H_2O-free reaction mixture ($N_2O + O_2$) for 5 h. In this

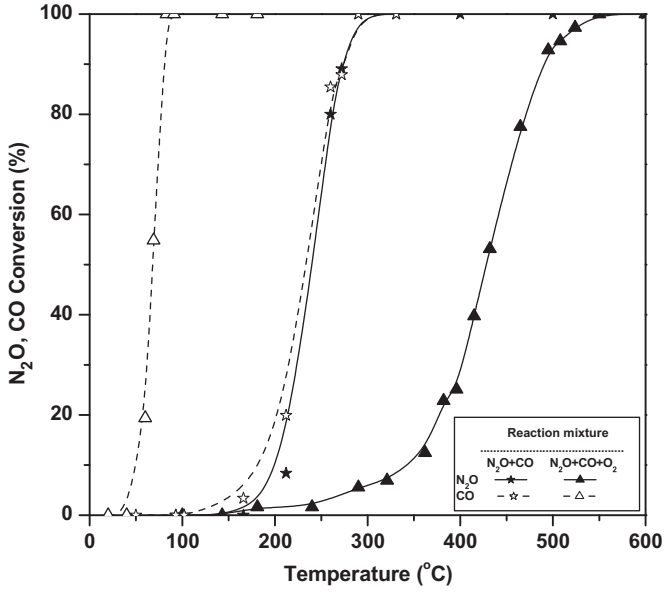

Fig. 4. Conversions of N_2O and CO during the N_2O reduction by CO in the absence or presence of O_2 over Pt/Al–CeLa monolithic sample. Reaction conditions: 0.1% N_2O, 0 or 2% O_2, 0.1% CO, GHSV = 10,000 h^{-1}.

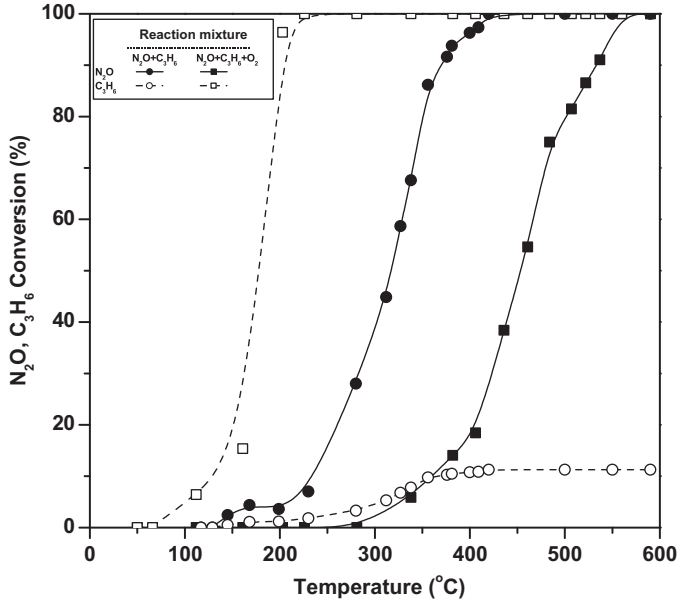

Fig. 5. Conversions of N_2O and C_3H_6 during the N_2O reduction by C_3H_6 in the absence or presence of O_2 over Pt/Al–CeLa monolithic sample. Reaction conditions: 0.1% N_2O, 0 or 2% O_2, 0.1% C_3H_6, GHSV = 10,000 h^{-1}.

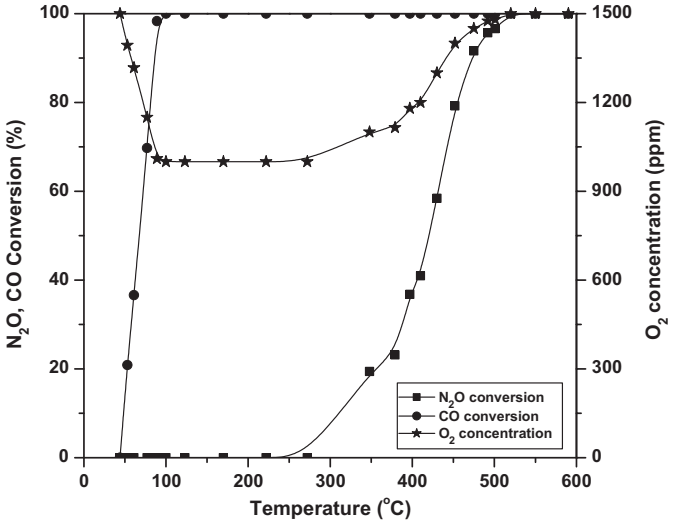

Fig. 6. Variation of O_2 concentration along with CO and N_2O conversions during the N_2O reduction by CO in the presence of O_2 over Pt/Al–CeLa monolithic sample. Reaction conditions: 0.1% N_2O, 0.15% O_2, 0.1% CO, GHSV = 10,000 h^{-1}.

first step, N_2O conversion remains constant and equal to 100%, indicating a good catalytic stability of Pt/Al–CeLa at dry conditions. However, when 3% H_2O is added in the feed stream, the N_2O conversion is gradually suppressed at ~22%, indicating the negative effect of steam on N_2O decomposition. After removing H_2O from feed stream, the de-N_2O performance is partially recovered (~75%). Complete restoration of the initial catalytic activity can be achieved after a short (~15 min) reduction with H_2 flow (Fig. 8). Similar steam inhibition effects have been reported for Ru/Al_2O_3 [45], CuO [22] and supported noble metal/transition metal oxides [35] catalyzed N_2O decomposition, which were attributed to competitive adsorption of H_2O and N_2O. Analogous steam-induced inhibition has also been observed during NO reduction by C_3H_8 over Rh/Al_2O_3, ascribed to the oxidation of Rh sites by H_2O adsorption [44]. Considering, in the present case, that the initial de-N_2O efficiency is not completely restored after water removal from the feed stream, it should be reasonably argued that the inhibition effect of water

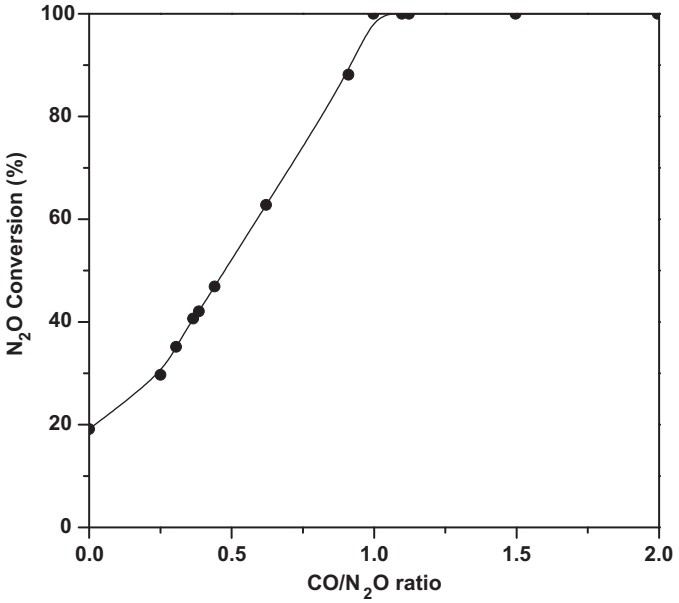

Fig. 7. N_2O conversion as a function of CO/N_2O ratio at 330 °C over Pt/Al–CeLa monolithic sample. Reaction conditions: 0.4% N_2O, 0–0.8% CO, GHSV = 10,000 h^{-1}.

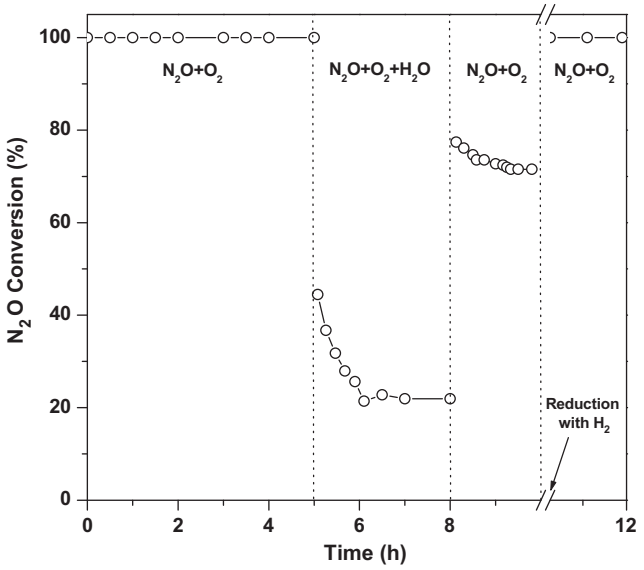

Fig. 8. Effect of water on N_2O conversion at 500 °C over Pt/Al–CeLa monolithic sample. Reaction conditions: 0.1% N_2O, 2% O_2, 0 or 3% H_2O, GHSV = 10,000 h^{-1}.

could not be solely attributed to competitive adsorption of N_2O and H_2O but also to permanent modification of Pt sites' activity. Given that reduced sites (Pt^0) are more active than oxidized sites ($Pt^{\delta+}$) for N_2O decomposition [45], an oxidation of Pt sites by H_2O may occur, which is consistent to the observed activity restoration after H_2 reduction.

It is generally accepted in the literature that the dominant path for N_2O elimination over Pt-group metals proceeds *via* the dissociative adsorption of N_2O molecule ($N_2O(g) \rightarrow N_2(g) + O_{ads}$) [*e.g.* 21, 46–51], with the removal of strongly adsorbed O_{ads} to be crucial for active sites regeneration. This mechanism is still at work even under the presence of a reducing agent [46,47] or under O_2 rich conditions [48–50]. In the latter case the dissociative chemisorption of O_2 seems to be more pronounced than that of N_2O at low and intermediate temperatures [*e.g.* 51]. The O_{ads} fragments of N_2O and/or O_2 dissociation are strongly adsorbed on active metal sites, inhibiting the de-N_2O reaction progress. In that case the role of a reducing agent is the scavenging of O_{ads} species liberating active sites for further N_2O decomposition [21]. Our aforementioned findings on Pt/Al_2O_3 and REOs-modified Pt/Al_2O_3 catalysts (Figs. 1–7) strongly corroborate all these mechanistic aspects as already analyzed in detail. The only point remaining to be interpreted is the REOs-induced substantial promotion of the de-N_2O activity of Pt sites. This point is examined below based on *in situ* DRIFTS studies.

3.5. Surface chemistry elucidation by in situ DRIFTS studies

The modifications induced by lanthanide elements (CeO_2 and La_2O_3) on the surface behavior of Pt/Al_2O_3 catalysts were evaluated by means of *in situ* DRIFT spectroscopy using CO as a probe molecule. This is because N_2O adsorption results in a hardly detected ad-species, in opposite to CO which is often used as a powerful probe molecule for evaluation of surface properties.

Fig. 9 depicts the IR spectra of adsorbed species obtained in the C—O stretching frequency region (2200–1700 cm^{-1}) over unmodified Pt/Al catalyst following CO expose to room temperature (25 °C) and then stepwise heating to 450 °C under He flow. Adsorption of CO at 25 °C produce two overlapping bands at 2084 and 2070 cm^{-1} in the ν(CO) stretching region, whereas in the low frequency region, located below 1700 cm^{-1} (not shown for clarity), several low intensity bands due to carbonates and/or carboxylates are observed.

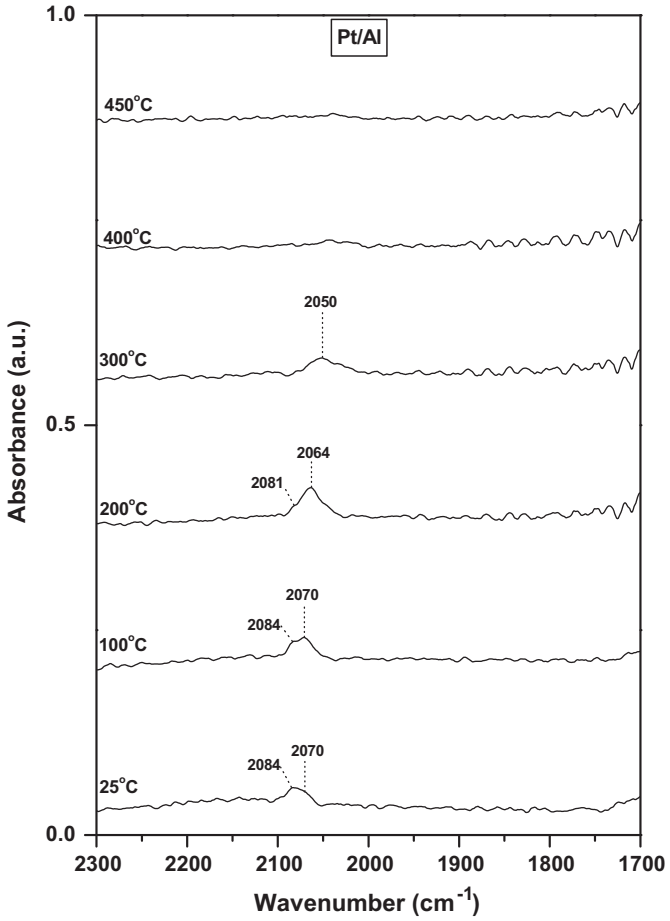

Fig. 9. DRIFT spectra of Pt/Al catalysts following CO adsorption at 25 °C and subsequent stepwise heating under He flow. FT-IR chamber feed: 0.5% CO; total flow 80 cm^3/min.

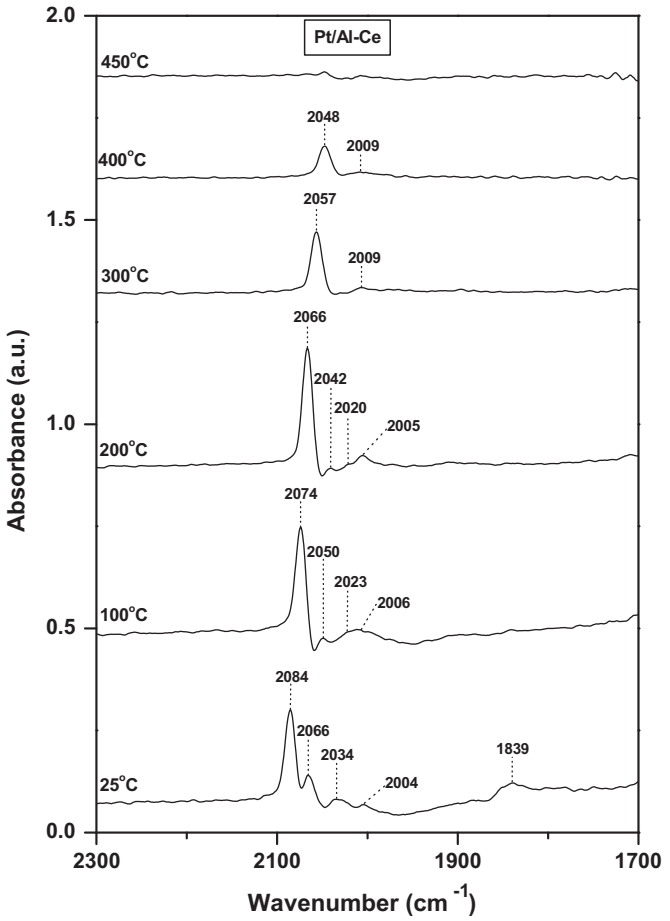

Fig. 10. DRIFT spectra of Pt/Al–Ce catalysts following CO adsorption at 25 °C and subsequent stepwise heating under He flow. FT-IR chamber feed: 0.5% CO; total flow: 80 cm^3/min.

The band at 2084 cm^{-1} is usually assigned to linearly bonded CO species on partially oxidized Pt sites ($Pt^{\delta+}$), whereas the band at 2070 cm^{-1} to linear CO on reduced Pt sites (Pt^0) [52]. However, taking into account that Pt/Al_2O_3 catalyst has been reduced with 20% hydrogen at 400 °C before CO adsorption, the assignment of the band at 2084 cm^{-1} to CO on oxidized Pt sites is not consistent to the reduction pretreatment. Consequently, the bands at 2084 cm^{-1} is assigned to CO linearly bound to the terrace sites of Pt particles, while the low energy band at 2070 cm^{-1} to carbonyl species adsorbed at the step sites of metallic Pt, in agreement with earlier IR studies concerning CO adsorption over pre-reduced or pre-oxidized Pt/Al_2O_3 catalysts [53–55]. It is worth noticing that temperature increase from 25 to 300 °C results in the progressive decrease in the intensity of the band assigned to carbonyl species on terrace sites (2084 cm^{-1}), while the band corresponding to CO on step sites (2070 cm^{-1}) gains in intensity until to 200 °C and then starts to attenuate, shifted at the same time to lower frequency. This possibly indicates a transfer in intensity from the CO band at terrace sites to CO on step sites, implying a redistribution of CO adsorbed species with temperature [54,55] or a CO-induced rearrangement of Pt particles [56]. The progressive shift of the CO band from 2070 cm^{-1} at 25 °C to 2050 cm^{-1} at 300 °C is consistent to the decreased dipole–dipole coupling between CO molecules as its surface coverage is decreased [54].

Figs. 10 and 11 depict the corresponding spectra acquired over the Pt/Al–Ce and Pt/Al–CeLa catalysts, respectively. Qualitatively similar spectra have been obtained in both catalysts, indicating that cerium oxide is crucial to the observed surface behavior modifications in respect to REOs-free Pt/Al catalyst (Fig. 9), showing that the observed differences among the surface behavior of REOs-modified and REOs-free catalysts can be mainly ascribed to the cerium oxide. These differences, reflecting the effect of lanthanides on Pt surface chemistry, are summarized as follows:

(i) Adsorption of CO at room temperature over REOs-promoted Pt/Al–Ce and Pt/Al–CeLa catalysts results in a significant higher intensity of linearly bonded CO bands at terrace (2084 cm^{-1}) and step (2070 cm^{-1}) sites, compared to the corresponding over REOs-free Pt/Al catalyst. This finding is directly related with the higher population of Pt surface sites (dispersion) over the CeO_2-enriched (Pt/Al–Ce) and $CeO_2 + La_2O_3$-enriched (Pt/Al–CeLa) catalysts, implying this way the pronounced effect of lanthanide elements on Pt dispersion; 81 and 93% over Pt/Al–Ce and Pt/Al–CeLa, respectively, in contrast to 14% over unmodified Pt/Al catalyst (Table 1). This argument is consistent to the appearance of the band at 1839 cm^{-1} (discussed below) only on REOs-modified samples; this band contributes less than 5% to the overall adsorption thus detected only on highly dispersed Pt samples [30].

(ii) Modification of Al_2O_3 support by CeO_2-based oxides (Figs. 10 and 11) results in the development of new overlapping bands in the 2035–1995 cm^{-1} region as well as of a band at 1839 cm^{-1}. The band at 1839 cm^{-1} is characteristic of bridged-bonded CO on reduced Pt sites [30,31], whereas the overlapping bands located in the 2035–1995 cm^{-1} region could be attributed to CO species adsorbed on metal sites with

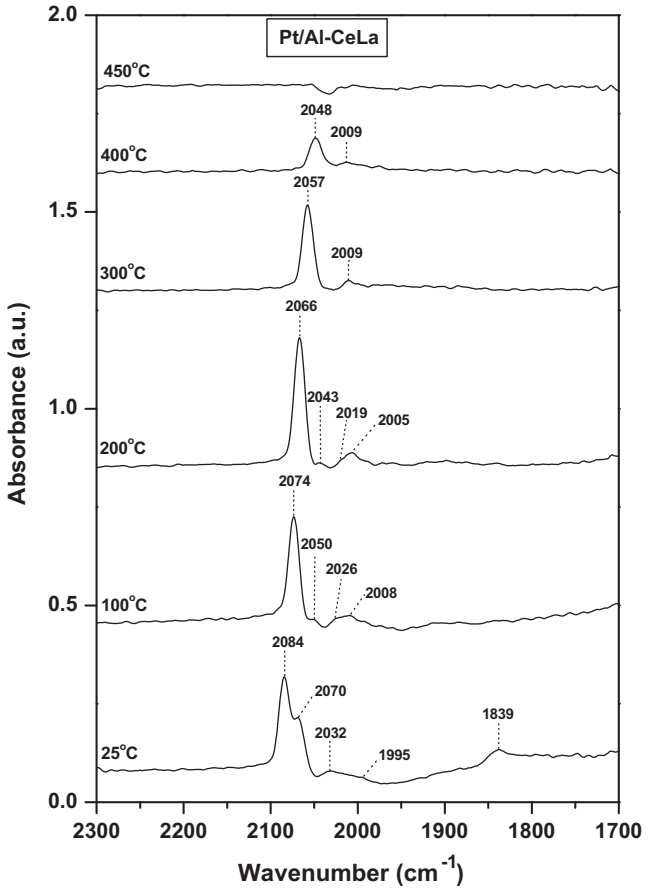

Fig. 11. DRIFT spectra of Pt/Al–CeLa catalysts following CO adsorption at 25 °C and subsequent stepwise heating under He flow. FT-IR chamber feed: 0.5% CO; total flow: 80 cm^3/min.

exceptional electron donating properties [57,58]. The development of such electron enriched sites in 2035–1995 cm^{-1} region is consistent to the appearance of bridged-bonded CO species at 1839 cm^{-1}, which is an indicator of an increased electron density of metal particles [30]. Given that the aforementioned bands were observed only on promoted catalysts, it should be argued that these bands are associated with Pt sites directly affected by REOs. Thus, the bands at 2035–1995 cm^{-1} and 1839 cm^{-1} should be attributed to CO species adsorbed on metal–support interfacial sites, which are strongly influenced by Ce^{3+} and/or La^{2+} promoter species. In consistent with this argument the low frequency bands at *ca.* 2035 cm^{-1} obtained during CO adsorption over Pt/CeO_2 [57] or Pd/CeO_2 [58] catalysts have been attributed to CO species over reduced metal sites with strong Ce^{3+} interaction. In accordance to Yee et al. [57] such electron enriched sites would be located on atomically rough parts of the surface or on isolated corner sites where dipolar coupling interactions are minimized; such sites favor the π-bonding with adsorbed CO thus shifting ν(CO) to lower frequencies [57].

3.6. Mode of action of REOs on N_2O decomposition

The results in Figs 1 and 2 clearly demonstrated that the N_2O decomposition over Pt-based catalysts is greatly affected by the incorporation of lanthanides on Al_2O_3 support. To explain this pronounced effect, it is necessary to take into consideration the generally accepted mechanism for N_2O elimination over noble metals catalysts, described with the following elementary steps [2,47]:

$$N_2O(g) \rightarrow N_2O_{ads} \quad (1)$$

$$N_2O_{ads} \rightarrow N_2(g) + O_{ads} \quad (2)$$

$$2O_{ads} \rightarrow O_2(g) \quad (3)$$

The above mechanistic sequence, supported also by the present results, involves first the chemisorption of N_2O *via* its terminal N on catalytically active sites and consequently its scission to $N_2(g)$ and O_{ads}. The latter is favored by the charge transfer from catalysts' Fermi level to the antibonding orbitals (π^*) of N_2O, which in turn weakens the N—O bond [59]. Although in the above elementary steps the decomposition of N_2O_{ads} to $N_2(g)$ and O_{ads} is generally considered as the rate determining step, the "cleanup" of catalyst surface covered by strongly adsorbed O_{ads} is also a key step since it determines the available sites for N_2O chemisorption [9,21]; the self-poisoning of catalyst surface by adsorbed oxygen species as well as the pronounced effect of reducing agents by facilitating the removal of O_{ads} have been already addressed in the present study, upon the discussion of the results of Figs. 3–7.

Considering the above N_2O decomposition mechanism it is reasonable to suggest that de-N_2O catalytic activity should be strongly related with the available surface sites for N_2O chemisorption and the strength of this N_2O chemisorption bond with catalyst surface; the former is directly related with the scavenge of catalyst surface from strongly adsorbed O_{ads} while the latter with the electron density of metal active sites. Taking into account the aforementioned factors, the enhanced catalytic performance of our REOs-modified catalysts can be rationalized on the basis of DRIFTS data (Figs. 9–11), which demonstrate that incorporation of CeO_2 and La_2O_3 oxides on Al_2O_3 support results in both (i) significant increase of Pt dispersion and (ii) Pt sites with exceptional electron density, located on the metal–support interfacial area.

The above beneficial effects of REOs are in line with their well established acid–base and redox properties, acting as oxygen buffer by storing/releasing oxygen depending on the ambient oxidizing/reducing conditions [29]. This superior oxygen storage capacity, induced by oxygen vacancies at the metal–support interface, can in turn influence the mobility of surface oxygen atoms and thus the electronic and chemisorptive properties of metal particles located at the metal–support interface [26–31]. In this context, mutual interactions between Ce-based oxides and metal particles have been considered for the activation of electron-acceptor adsorbates (such as NO or N_2O) on highly reducible sites at metal–support interface [29,31].

4. Conclusions

In the present study the pronounced effect of CeO_2 and La_2O_3 additives as Al_2O_3 support modifiers during the N_2O decomposition/reduction over Pt-based honeycomb monoliths was clearly demonstrated. It was found that the catalytic performance of Pt/Al_2O_3 monoliths can be remarkable enhanced by the modification of Al_2O_3 support by REOs leading to complete conversion of N_2O at temperatures as low as ~450 °C even in the presence of O_2. Under reducing conditions, the N_2O conversion is strongly enhanced by C_3H_6 and especially by CO, since reducing agents facilitate the removal of strongly adsorbed oxygen species. On the other hand under O_2 excess conditions a slight inhibition is induced by reducing agents due to competitive adsorption of reactants. Water has a detrimental influence on N_2O decomposition, attributed to the competitive adsorption of H_2O and N_2O as well as to its permanent effect on Pt oxidation state. The evolution of surface behavior of un-promoted and REOs-promoted catalysts my

means of *in situ* diffuse reflectance infrared Fourier transform spectroscopy (DRIFTS) studies, using CO as a probe molecule, revealed that the superior catalytic performance of promoted samples can be mainly attributed to the increase of available metal surface area as well as to the development of new Pt sites with exceptional electron density, located on the metal–support interfacial area.

Acknowledgments

Financial support by the program "THALIS" implemented within the framework of Education and Lifelong Learning Operational Programme, co-financed by the Hellenic Ministry of Education, Lifelong Learning and Religious Affairs and the European Social Fund is gratefully acknowledged. Partial financial support from the Research Committee of the Technical University of Crete is also acknowledged.

References

[1] J. Pérez-Ramírez, F. Kapteijn, K. Schöffel, J.A. Moulijn, Applied Catalysis B 44 (2003) 117.
[2] F. Kapteijn, J. Rodriquez-Mirasol, J.A. Moulijn, Applied Catalysis B 9 (1996) 25.
[3] G. Centi, S. Perathoner, F. Vazzana, M. Marella, M. Tomaselli, M. Mantegazza, Advances in Environmental Research (2000) 325.
[4] J. Pérez-Ramírez, Applied Catalysis B 70 (2007) 31.
[5] G. Centi, S. Perathoner, Z.S. Rak, Applied Catalysis B 41 (2003) 143.
[6] D.J. Wuebbles, Science 326 (2009) 56.
[7] A.R. Ravishankara, J.S. Daniel, R.W. Portmann, Science 326 (2009) 123.
[8] J.P. Dacquin, C. Dujardin, P. Granger, Catalysis Today 137 (2008) 390.
[9] R. Burch, S.T. Daniells, J.P. Breen, P. Hu, Journal of Catalysis 224 (2004) 252.
[10] S. Imamura, R. Hamada, Y. Saito, K. Hashimoto, H. Jindai, Journal of Molecular Catalysis A 139 (1999) 55.
[11] C. Ohnishi, S. Iwamoto, M. Inoue, Chemical Engineering Science 63 (2008) 5076.
[12] G.E. Marnellos, E.A. Efthimiadis, I.A. Vasalos, Applied Catalysis B 46 (2003) 523.
[13] S. Parres-Esclapez, M.J. Illán-Gómez, C. Salinas-Martínez de Lecea, A. Bueno-López, Applied Catalysis B 96 (2010) 370.
[14] G. Giecko, T. Borowiecki, W. Gac, J. Kruk, Catalysis Today 137 (2008) 403.
[15] L. Obalová, K. Pacultová, J. Balabánová, K. Jirátová, Z. Bastl, M. Valášková, Z. Lacný, F. Kovanda, Catalysis Today 119 (2007) 233.
[16] Li Xue, C. Zhang, H. He, Y. Teraoka, Applied Catalysis B 75 (2007) 167.
[17] R. Nunzio, F. Debora, S. Guido, S. Vito, Catalysis Today 119 (2007) 228.
[18] M.N. Debbagh, C. Salinas Martínez de Lecea, J. Pérez-Ramírez, Applied Catalysis B 70 (2007) 335.
[19] P.J. Smeets, M.H. Groothaert, R.M. van Teeffelen, H. Leeman, E.J.M. Hensen, R.A. Schoonheydt, Journal of Catalysis 245 (2007) 358.
[20] G. Centi, A. Galli, B. Montanari, S. Peranthoner, A. Vaccari, Catalysis Today 35 (1997) 113.
[21] R. Burch, S.T. Daniells, J.P. Breen, P. Hu, Catalysis Letters 94 (2004) 103.
[22] N. Pasha, N. Lingaiah, P.S.S. Reddy, P.S.S. Prasad, Catalysis Letters 118 (2007) 64.
[23] F. Zasada, P. Stelmachowski, G. Maniak, J.-F. Paul, A. Kotarba, Z. Sojka, Catalysis Letters 127 (2009) 126.
[24] P. Stelmachowski, G. Maniak, A. Kotarba, Z. Sojka, Catalysis Communications 10 (2009) 1062.
[25] J. Haber, M. Nattich, T. Machej, Applied Catalysis B 77 (2008) 278.
[26] P. Granger, G. Leclercq, Journal of Physical Chemistry C 111 (2007) 9905.
[27] X. Li, C. Zhang, H. He, Y. Teraoka, Applied Catalysis B 75 (2007) 167.
[28] J. Pérez-Ramírez, F. Kapteijn, Applied Catalysis B 47 (2004) 177.
[29] A. Trovarelli, Catalysis Reviews, Science and Engineering 38 (1996) 439.
[30] B.A. Riguetto, S. Damyanova, G. Gouliev, C.M.P. Marques, L. Petrov, J.M.C. Bueno, Journal of Physical Chemistry B 108 (2004) 5349.
[31] A. Martinez-Arias, J.M. Coronado, R. Cataluña, J.C. Conesa, J. Soria, Journal of Physical Chemistry B 102 (1998) 4357.
[32] V. Matsouka, M. Konsolakis, R.M. Lambert, I.V. Yentekakis, Applied Catalysis B 84 (2008) 715.
[33] J.C.S. Araujo, D. Zanchet, R. Rinaldi, U. Schuchardt, C.E. Hori, J.L.G. Fierro, J.M.C. Bueno, Applied Catalysis B 84 (2008) 552.
[34] A. Papavasiliou, A. Tsetsekou, V. Matsouka, M. Konsolakis, I.V. Yentekakis, Applied Catalysis A 382 (2010) 73.
[35] V. Boissel, S. Tahir, C.A. Koh, Applied Catalysis B 64 (2006) 234.
[36] S. Suárez, M. Yates, A.L. Petre, J.A. Martín, P. Avila, J. Blanco, Applied Catalysis B 64 (2006) 302.
[37] S. Suárez, C. Saiz, M. Yates, J.A. Martín, P. Avila, J. Blanco, Applied Catalysis B 55 (2005) 57.
[38] N. Russo, D. Mescia, D. Fino, G. Saracco, V. Specchia, Industrial and Engineering Chemistry Research 46 (2007) 4226.
[39] T. Zhou, L. Li, C. Jie, Q. Shen, Q. Xie, Z. Hao, Ceramics International 35 (2009) 3097.
[40] E. Ruiz-Martínez, J.M. Sánchez-Hervás, J. Otero-Ruiz, Applied Catalysis B 61 (2005) 306.
[41] A. Papavasiliou, A. Tsetsekou, V. Matsouka, M. Konsolakis, I.V. Yentekakis, N. Boukos, Applied Catalysis B 90 (2009) 162.
[42] J.-H. Park, J.-H. Choung, I.-S. Nam, S.-W. Ham, Applied Catalysis B 78 (2008) 342.
[43] V.G. Komvokis, M. Marti, A. Delimitis, I.A. Vasalos, K.S. Triantafyllidis, Applied Catalysis B 103 (2011) 62.
[44] G. Pekridis, N. Kaklidis, V. Komvokis, C. Athanasiou, M. Konsolakis, I.V. Yentekakis, G.E. Marnellos, Journal of Physical Chemistry A 114 (2010) 3969.
[45] V.G. Komvokis, G.E. Marnellos, I.A. Vasalos, K.S. Triantafyllidis, Applied Catalysis B 89 (2009) 627.
[46] A. de Lucas-Consuegra, F. Dorado, C. Jiménez-Borja, J.L. Valverde, Applied Catalysis B 78 (2008) 222.
[47] P. Granger, P. Malfoy, P. Esteves, L. Leclercq, G. Leclercq, Journal of Catalysis 187 (1999) 321.
[48] S.C. Christoforou, E.A. Efthimiadis, I.A. Vasalos, Catalysis Letters 79 (2002) 137.
[49] K. Pacultová, L. Obalová, F. Kovanda, K. Jirátová, Catalysis Today 137 (2008) 385.
[50] N.W. Cant, D.C. Chambers, Y. Yoshinaga, Catalysis Communications 5 (2004) 625.
[51] R.W. McCabe, Ch. Wong, Journal of Catalysis 121 (1990) 422.
[52] P.-A. Carlsson, L. Österlunda, P. Thormählen, A. Palmqvist, E. Fridell, J. Jansson, M. Skoglundh, Journal of Catalysis 226 (2004) 422.
[53] K. Tanaka, J.M. White, Journal of Catalysis 79 (1983) 81.
[54] M. Primet, Journal of Catalysis 88 (1984) 273.
[55] P. Panagiotopoulou, D.I. Kondarides, Journal of Catalysis 260 (2008) 141.
[56] J. Rasko, Journal of Catalysis 217 (2003) 478.
[57] A. Yee, S.J. Morrison, H. Idriss, Journal of Catalysis 191 (2000) 30.
[58] A. Bensalem, J.-C. Muller, D. Tessier, F. Bozon-Verduraz, Journal of the Chemical Society, Faraday Transactions 92 (1996) 3233.
[59] W.B. Tolman, Angewandte Chemie International Edition 49 (2010) 1018.